J. Fluid Mech. (1985), *vol.* 156, *pp.* 83–100
Printed in Great Britain

On the stability of Poiseuille–Couette flow: a bifurcation from infinity

By S. J. COWLEY AND F. T. SMITH
Mathematics Department, University College, Gower Street, London WC1E 6BT

(Received 30 January 1984 and in revised form 2 October 1984)

The linear and weakly nonlinear stability of Poiseuille–Couette flow is considered for various values of the relative wall velocity $2u_w$. An account is given first of the asymptotic upper and lower branches of the linear neutral curve(s), followed by their disappearance, as u_w is increased. *Two* main (and one minor) neutral curves are found to exist for smaller $O(1)$ (or lesser) values of u_w, then one for moderate $O(1)$ values of u_w, and none for larger $O(1)$ values of u_w. The cut-off velocity at which each main neutral curve disappears is determined, and in each case the whole neutral curve for u_w just below the cut-off value is determined in closed form. Secondly, weakly nonlinear solutions are found to bifurcate subcritically from the neutral curve for u_w just below cut-off, but to 'bifurcate from infinity' just above cut-off. This identifies a minimum threshold amplitude at the entry to the regime where no linear neutral curve exists.

1. Introduction

Although plane Poiseuille channel flow and plane Couette flow are observable experimentally at lower Reynolds numbers, both flows become unstable at higher Reynolds numbers, for different reasons. Many aspects of plane Poiseuille flow (PPF) instability are known and have been reviewed by Herbert (1981*a*), Stuart (1981) and in Orszag & Kell's (1980) introduction, for example. In summary, for Reynolds numbers $R \leqslant R_c$ (≈ 5772) PPF is linearly stable, while for $R > R_c$ certain infinitesimal disturbances grow (Heisenberg 1924; Orszag 1971). Weakly nonlinear analysis then shows that at $R = R_c$ there is a subcritical bifurcation of a two-dimensional progressive-wave finite-amplitude solution (Stuart 1960; Reynolds & Potter 1967; Stewartson & Stuart 1971). Such solutions at non-small amplitudes have been found to varying degrees of approximation by Meksyn & Stuart (1951), Zahn *et al.* (1974), Herbert (1976) and others. In the parameter space formed by Reynolds number, wavenumber and amplitude, these two-dimensional waves map out a 'neutral' surface (Herbert 1977), a typical cross-section of which is illustrated in figure 1 for a fixed $R < R_c$. The 'lower' branch (LB) of this surface is unstable to two-dimensional disturbances, while the upper branch (UB) is stable. For $R < R_G \approx 2935$, no finite-amplitude two-dimensional periodic states exist, and all two-dimensional disturbances are believed to decay (Orszag & Kells 1980).

The LB neutral solution gives a threshold amplitude for $R \geqslant R_G$, below which two-dimensional disturbances decay, and above which disturbances force the flow to snap through to the appropriate UB solution. On the other hand, these UB solutions themselves are unstable to three-dimensional disturbances according to computations by Orszag & Kells (1980) (see also Orszag & Patera 1980; Herbert 1981*b*). Further, these three-dimensional instabilities exist for $R < R_G$, in fact down to Reynolds

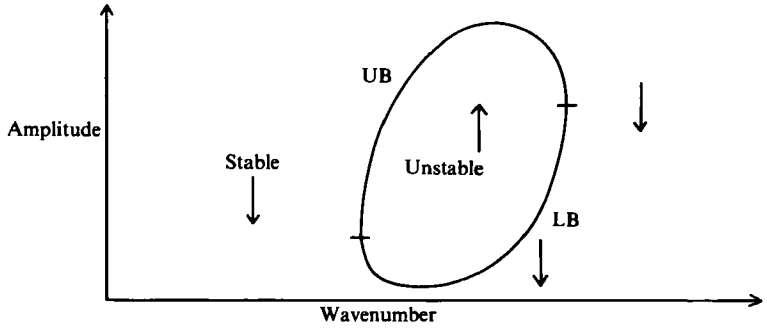

FIGURE 1. A subcritical section of the neutral surface for PPF, and typical of Reynolds numbers R where $R_G < R < R_c$. The stability of the solutions to two-dimensional disturbances is indicated by the arrows.

numbers as low as about 1000. This seems in good agreement with experiment. Recently, Herbert (1983*a*, *b*) has examined the stability of the LB nonlinear solutions to three-dimensional disturbances, finding another critical Reynolds number (below R_c) beneath which certain ones grow more rapidly than the two-dimensional ones. Mr A. Bernoff (private communication) has noted that at this critical Reynolds number a bifurcating solution is likely, and the lowest R at which this or a similar three-dimensional solution exists could be related to the lowest Reynolds number at which PPF is unstable to large-amplitude disturbances.

In contrast, the understanding of plane Couette flow (CF) stability is far from complete, owing mainly to the lack of a linear neutral curve. Romanov (1973) has indicated a proof that CF is linearly stable at all R, but attempts to find two-dimensional nonlinear forms, to tie in with the experimental instability, have had mixed success. Thus the forms of Ellingsen, Gjevik & Palm (1970), Coffee (1977), Itoh (1977) and Davey (1978*a*) came from expanding about the slowest decaying linear mode. Davey (1978*a*) among others notes the difficulties of this non-asymptotic procedure, and Rosenblat & Davis' (1979) model problem brings that further into question. Also, Orszag & Kells' computations suggest that such nonlinear solutions might be spurious. Therefore it seems possible that CF is stable to all nonlinear *two*-dimensional disturbances. *Three*-dimensional effects, however, render CF nonlinearly unstable, according to Orszag & Kells, at Reynolds numbers of order 1000.

Similar difficulties with the nonlinear stability question exist in Hagen–Poiseuille flow through a circular pipe and other flows linearly stable at all R, although Smith & Bodonyi (1982) have recently identified part of the nonlinear neutral surface for Hagen–Poiseuille flow, at large R. It is likely that these nonlinear finite-amplitude states give unstable threshold amplitudes for a fixed wavelength. The Smith & Bodonyi analysis could not identify those nonlinear solutions with the smallest pressure amplitude, but did indicate that their wavelength is $O(R)$, with axial velocity profiles that are distinctly non-parabolic.

The current aim is to treat flows that are linearly stable at all R by an asymptotic method perhaps complementary to Smith & Bodonyi's. Asymptotic or multistructured analysis is very helpful, we should perhaps recall, because it provides useful physical insight, structural and theoretical understanding, numerical guidelines, a different firm perspective and, not least, an easier access to the all-important nonlinear regime. Moreover, it points to alternative more efficient numerical methods (e.g. Smith, Papageorgiou & Elliott 1984) and its predictions tend to 'work' even at low

subcritical values of R: see the last-named paper and references therein. Below, rather than studying CF we examine the linear combination of CF with PPF, produced in a channel by an applied pressure gradient and walls moving at different velocities, say (without loss of generality) with the same speed but in opposite directions. The linear stability of this plane 'Poiseuille–Couette' flow (PPCF) has been studied previously by Potter (1966), Hains (1967) and Reynolds & Potter (1967). Heuristically, as in Heisenberg (1924) and Lin (1945), Potter (1966) demonstrated that above a certain 'cut-off' value of the non-dimensional wall velocity u_w no neutral curve could be found. Numerical solutions of the Orr–Sommerfeld equation by Hains and Reynolds & Potter confirmed this result: more comments are given later.

First below, in §2, the large-Reynolds-number forms of the linear neutral curve are derived for u_w less than cut-off. Unlike in PPF, for $u_w = O(1)$ the neutral and unstable wavelengths in PPCF are very long, $O(R)$. The Appendix shows, for those interested, the transition to PPF behaviour as u_w decreases towards zero and, further, that there are sometimes *two* or *three* neutral curves. The work in §2 determines the two cut-off values of u_w at which the two main neutral curves disappear, the precise nature of that disappearance being given subsequently in §3. Also in §3, weakly nonlinear effects are considered for u_w close to a cut-off value. For infinitesimal disturbances, with u_w just below cut-off, an analytic expression for the *whole* (disappearing) linear neutral curve is obtained. For u_w above cut-off the neutral states have finite amplitudes, and because these states prove to be unstable this identifies a *minimum threshold amplitude* for nonlinear two-dimensional disturbances. Finally, further comments are made in §4.

2. Wall velocities less than cut-off

The Cartesian coordinates, time, pressure and velocities are denoted by $b\boldsymbol{x}$, $bU_m^{-1}t$, $\rho U_m^2 p$ and $U_m \boldsymbol{u}$ respectively (figure 2), where b is the channel half-width, ρ is the incompressible fluid's density and U_m is the mean velocity. Hence the non-dimensional Navier–Stokes and continuity equations read

$$\boldsymbol{u}_t + (\boldsymbol{u}\cdot\nabla)\boldsymbol{u} = -\nabla p + R^{-1}\nabla^2\boldsymbol{u}, \quad \nabla\cdot\boldsymbol{u} = 0, \tag{2.1a,b}$$

where $R = U_m b/\nu$, ν is the kinematic viscosity; and the boundary conditions

$$u = -u_w, \quad v = 0 \quad \text{on } y = -1, \tag{2.2a}$$

$$u = u_w, \quad v = 0 \quad \text{on } y = 1 \tag{2.2b}$$

hold, with $2u_w$ being the relative wall velocity. The unperturbed-flow solution is

$$u = u_0(y) = \tfrac{3}{2}(1-y^2) + u_w y, \quad v = 0, \quad p = p_0(x) = -3xR^{-1}. \tag{2.3}$$

Note that for PPF the critical Reynolds number R_c here is 3848 instead of the better-known value of 5772.

One neutral curve for infinitesimal disturbances to (2.3) is given by Potter (1966), Hains (1967) and Reynolds & Potter (1967) for various u_w. For $u_w = 0$ (PPF) it is known that, if the disturbance wavenumber is α, then $\alpha R^{\frac{1}{7}}$ and $\alpha R^{\frac{1}{11}}$ tend to constants on the lower and upper branches respectively for large R. In the Appendix we study how these properties change as u_w increases through the distinguished scales $R^{-\frac{1}{7}}$, $R^{-\frac{4}{15}}$, $R^{-\frac{1}{11}}$ and $R^{-\frac{4}{13}}$, deducing that when u_w reaches $O(1)$ both the upper and lower branches have $\alpha R \sim$ constant (and at least *two* neutral curves exist then). Similar changes occur in pipe flows as the aspect ratio is decreased (Smith 1979), while the lower branch

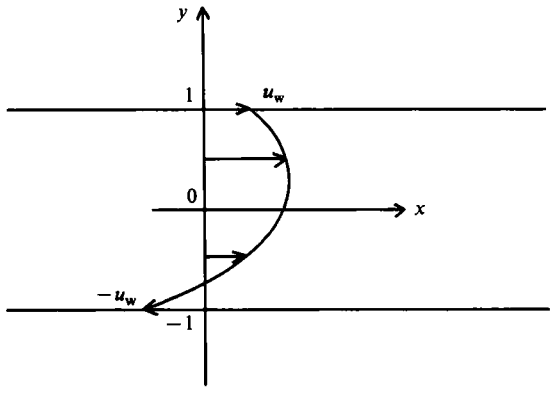

FIGURE 2. Diagram illustrating coordinate axes and non-dimensionalization.

for the odd neutral mode of the Bickley jet also produces such long $O(R)$ lengthscales, as does rotating pipe flow (e.g. Mackrodt 1976).

The present reason for examining the asymptotic behaviour is that at a 'cut-off' wall velocity, $u_w = u_w^*$, say, the two branches are expected to coalesce, so that u_w^* is determined just by the asymptotic problem. As usual, disturbances harmonic in x, t, and of amplitude δ and phase speed c, are sought:

$$[u-u_0, v, p-p_0] = \delta e^{i\alpha(x-ct)} [\tilde{u}, \tilde{v}, \tilde{p}](y). \tag{2.4}$$

At large R the form

$$[\alpha R, c, \tilde{u}, \tilde{v}] = [\lambda_0^{-1}, c_0, \phi_0'(y), -i\alpha\phi_0(y)] + o(1) \tag{2.5}$$

is expected, where ϕ_0 is the non-harmonic component of the stream function. From (2.4), (2.5) and (2.1), and provided δ is smaller than any negative power of R, the leading-order equation is

$$i\lambda_0 \phi_0^{IV} + (u_0 - c_0)\phi_0'' - u_0''\phi_0 = 0, \tag{2.6a}$$

a long-wave version of the Orr–Sommerfeld equation. The boundary conditions here are

$$\phi_0 = \phi_0' = 0 \quad \text{on } y = -1, 1. \tag{2.6b}$$

Equations (2.6a, b) then pose an eigenvalue problem for c_0 in terms of λ_0 and u_w. The values of λ_0 for which c_0 is real define the asymptotes of the neutral curves.

Equations (2.6) were solved numerically by an adaptation of Smith's (1974) finite-difference method. A variable step length Δy in y was used to cluster the gridpoints close to the walls, where Δy was varied from 10^{-6} to 5×10^{-5}, while at the centre it was typically 5×10^{-3}. Up to 3001 gridpoints were spread across the channel. The method was confirmed to have $O(h^2)$ accuracy, and Richardson extrapolation was used to improve this to $O(h^4)$ for certain of the results.

In figures 3(a, b) the limiting wavespeed c_0 and scaled wavelength λ_0 are plotted for the neutral curve found by Hains (1967) and Potter & Reynolds (1967). The upper and lower branches are marked according to their normal linear definitions, along with the lower-branch asymptote, from the Appendix. Despite first appearances, $c_0 \to 0$ from above as $u_w \to 0$ on the upper branch. This is illustrated more clearly in the enlargement in figure 4(a) of an area within the dotted circle of figure 3(a). The

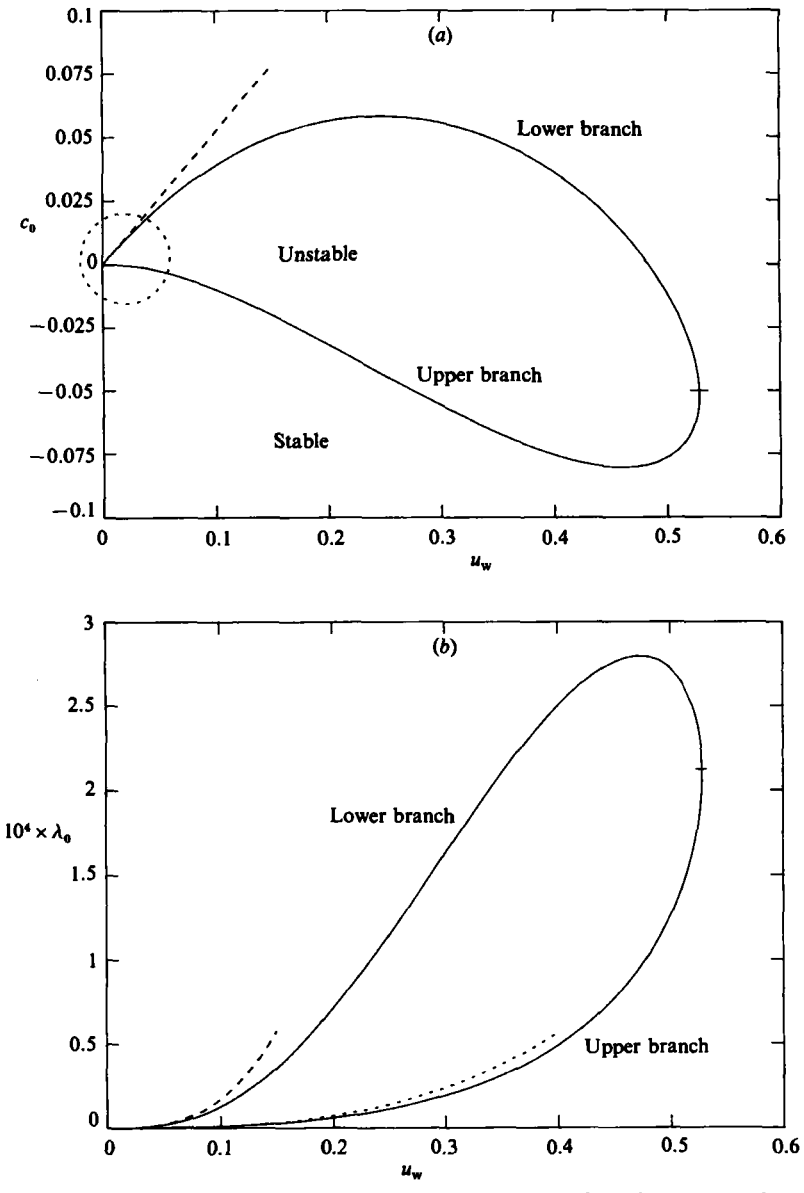

FIGURE 3. Plot of (*a*) wavespeed and (*b*) scaled wavelength versus wall velocity for mode M1; – – – –, asymptotes valid as $u_w \to 0$ (see Appendix).

upper branch of figure 3(*a*) is labelled M1 in figure 4(*a*). It asymptotes to 0+ along the dotted line as $u_w \to 0$: see Appendix. Also illustrated in figure 4(*a*), is a *second* neutral curve, which emerges for small values of u_w. This, with its unstable modes (M2), does not seem to have been identified before, probably because it exists only at quite large R. Moreover, the growth rates inside the second neutral curve are smaller than the original ones, so that these new modes seem of less physical importance. Figure 4(*b*) is a plot of the scaled wavelength against u_w for this second mode M2.

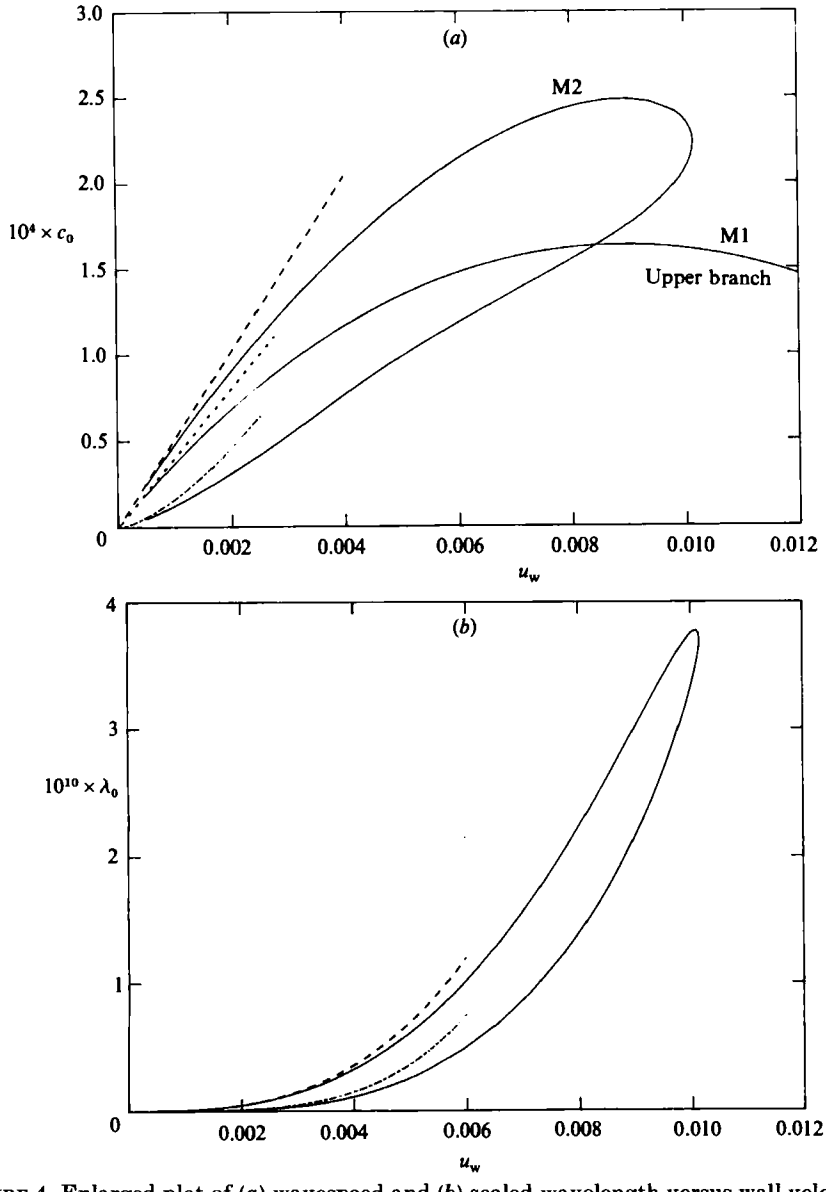

FIGURE 4. Enlarged plot of (*a*) wavespeed and (*b*) scaled wavelength versus wall velocity for mode M2 and the upper branch of M1 (wavespeed only); – – – –, ····, –·–·, asymptotes valid as $u_w \to 0$ (see Appendix).

Figures 3 and 4 show that for each neutral mode there exists a cut-off wall velocity u_w^* below which the neutral curve exists and above which it does not. A method explained in §3 gives the cut-off values:

$$u_w^* = 0.5279 \quad (\text{with } \lambda_0 = \lambda^* = 2.096 \times 10^{-4},\ c_0 = c^* = -0.0513)\ (\text{M1}), \qquad (2.7a)$$

$$u_w^* = 0.01020 \quad (\text{with } \lambda_0 = \lambda^* = 3.755 \times 10^{-10},\ c_0 = c^* = 2.2 \times 10^{-4})\ (\text{M2}). \qquad (2.7b)$$

A comparison with Reynolds & Potter's (1967) calculations is made in §3.

The above leads on to the investigation in §3 below of the complete disappearance of the neutral curve, and of weakly nonlinear effects, near the cut-off values $u_w = u_w^*$.

3. Linear and weakly nonlinear properties near cut-off

The key here is to scale the flow parameters so as to locate both the linear and weakly nonlinear neutral curves by use of a disturbance amplitude $a\delta$. We assume that $\delta \ll 1$, and then relate the other parameters to it. Weak nonlinearity results when a is $O(1)$, while the linear neutral curve is recovered for $a \to 0$.

Reynolds & Potter's calculations point to a subcritical Hopf bifurcation from the linear neutral curve, as in PPF, when R is close to R_c. Near the bifurcation point,

$$\Psi = \int_0^y u_0 \, \mathrm{d}y + \delta\Psi_0 + \delta^2\Psi_1 + \delta^3\Psi_2 + \ldots, \tag{3.1a}$$

$$c = c_0 + \delta c_1 + \delta^2 c_2 + \ldots, \tag{3.1b}$$

with c_n real: see e.g. Chen & Joseph (1973). The novelty here, however, is that αR is $O(1)$, from §2, and so

$$\lambda = (\alpha R)^{-1} = \lambda_0 + \delta\lambda_1 + \delta^2\lambda_2 + \ldots. \tag{3.1c}$$

It now remains to fix the orders of $u_w - u_w^*$, the slow-time variation, and α.

First, figures 3 and 4 indicate that a linear variation in c and λ leads to a quadratic variation in u_w when $u_w \to u_w^*$ (note that Chen & Joseph have $c_1 = \lambda_1 = 0$, and hence different scalings from those proposed here). Therefore we write

$$u_w = u_w^* + \delta^2 W. \tag{3.1d}$$

Next, as $u_w \to u_w^*$ the upper and lower branches join (figures 3*a*, 4*a*) and the form $\mathrm{Im}\,(c) \sim \text{constant}\,(\lambda_U - \lambda)(\lambda - \lambda_L)$ is anticipated, where λ_U and λ_L specify the upper and lower branches for a given u_w. Hence $\mathrm{Im}\,(c) = O(\delta^2)$ in effect for (3.1*d*), suggesting the scaled times

$$\tau = \alpha c t, \quad T = \alpha\delta^2 t. \tag{3.1e}$$

The fast time τ accounts for the basic harmonic variation, while the slow time T governs the disturbance growth. In (3.1*e*), $|c|$ replaces c if $c < 0$, but this only marginally alters details of the ensuing analysis.

The appropriate wavelength is fixed by streamwise diffusion, an $O(\alpha^2)$ relative effect ignored in §2, which implies the scaling

$$X = \alpha x, \quad \alpha = \delta\alpha_s. \tag{3.1f}$$

Here, incidentally, the unusual inclusion of streamwise diffusion effects, which fix a critical Reynolds number for u_w near u_w^* (see below), would require a slight modification to the 'pragmatic' approach of Smith *et al.* (1984).

Substitution of (3.1) into (2.1) and (2.2) then leads to the sequence of equations

$$\mathrm{L}\Psi_0 = 0, \tag{3.2a}$$

$$\mathrm{L}\Psi_1 = -c_1 \Psi_{0yy\tau} + \lambda_1 \Psi_{0yyyy} - \mathrm{J}(\Psi_0, \Psi_{0yy}), \tag{3.2b}$$

$$\begin{aligned}\mathrm{L}\Psi_2 = {} & -c_1 \Psi_{1yy\tau} + \lambda_1 \Psi_{1yyyy} - c_2 \Psi_{0yy\tau} + \lambda_2 \Psi_{0yyyy} \\ & - \alpha_s^2 (c_0 \Psi_{0XX\tau} + \hat{u}_0 \Psi_{0XXX} - 2\lambda_0 \Psi_{0XXyy}) \\ & - W\tilde{u}_0 \Psi_{0Xyy} - \Psi_{0yyT} - \mathrm{J}(\Psi_1, \Psi_{0yy}) - \mathrm{J}(\Psi_0, \Psi_{1yy}),\end{aligned} \tag{3.2c}$$

$$\Psi_j = (\Psi_j)_y = 0 \quad \text{on } y = \pm 1, \tag{3.2d}$$

where
$$\mathrm{L} \equiv \hat{u}_0 \partial_{yyX} + c_0 \partial_{yyT} - \hat{u}_{0yy} \partial_X - \lambda_0 \partial_{yyyy}, \tag{3.3a}$$
$$\mathrm{J}(\Psi, \Phi) \equiv \Psi_y \Phi_X - \Psi_X \Phi_y, \tag{3.3b}$$
$$\hat{u}_0(y) \equiv u_0(y) \quad \text{for } u_w = u_w^*, \quad \tilde{u}_0(y) \equiv y. \tag{3.3c}$$

Solutions are sought now with period 2π in X and τ:
$$\Psi_0 = (a(T) z_0 + \bar{a}(T) \bar{z}_0), \tag{3.4a}$$
where
$$z_0(\theta, y) = \mathrm{e}^{\mathrm{i}\theta} \phi_0(y), \quad \theta = X - \tau, \tag{3.4b}$$

$\phi_0(y)$ is as in (2.5) and a bar denotes the complex conjugate. From (3.4) and (3.2a), ϕ_0 satisfies
$$\mathrm{i}\lambda_0 \phi_0^{\mathrm{IV}} + (\hat{u}_0 - c_0) \phi_0'' - \hat{u}_{0yy} \phi_0 = 0, \tag{3.5a}$$
$$\phi_0 = \phi_0' = 0 \quad \text{on } y = \pm 1. \tag{3.5b}$$

It follows that $\lambda_0 = \lambda^*$ and $c_0 = c^*$ as in (2.7a,b).

A solution for Ψ_1 can be found only if (3.2b) satisfies a solvability condition. We therefore introduce the inner product
$$[\beta, \gamma] = \frac{1}{4\pi^2} \int_0^{2\pi} \mathrm{d}X \int_0^{2\pi} \mathrm{d}\tau \langle \beta, \gamma \rangle, \tag{3.6a}$$
where
$$\langle \beta, \gamma \rangle = \int_{-1}^{1} \beta \bar{\gamma} \, \mathrm{d}y, \tag{3.6b}$$

and denote by L^+ and z_0^+ ($= \mathrm{e}^{\mathrm{i}\theta} \phi_0^+$) respectively the operator and eigenfunction adjoint to L and z_0 relative to (3.6). Then the Fredholm alternative for (3.2b) yields the solvability condition
$$[c_1 \Psi_{0yyT} + \lambda_1 \Psi_{0yyyy} - \mathrm{J}(\Psi_0, \Psi_{0yy}), z_0^+] = 0, \tag{3.7}$$
or, in view of (3.4) and (3.6),
$$c_1 = p_2 \lambda_1, \tag{3.8a}$$
where
$$p_1 p_2 = \mathrm{i} \langle \phi_0^{\mathrm{IV}}, \phi_0^+ \rangle, \quad p_1 = \langle \phi_0'', \phi_0^+ \rangle. \tag{3.8b}$$

If u_w^* is a cut-off wall velocity (3.1b–d) imply that c_1 and λ_1 must be non-zero, and so from (3.8a) p_2 must be real. The calculation method for u_w^* and c^* used this property and the repeated secant method. Because no eigensolutions exist above cut-off, convergence was ensured by regarding u_w as a function of c_0, rather than vice versa.

From (3.8a) and (3.4) the solution to (3.2b) takes the form
$$\Psi_1 = \lambda_1 (a \, \mathrm{e}^{\mathrm{i}\theta} \phi_{11}(y) + \mathrm{c.c.}) + ((a\bar{a}\phi_{12}(y) + a^2 \mathrm{e}^{2\mathrm{i}\theta} \phi_{13}(y)) + \mathrm{c.c.}), \tag{3.9}$$
where c.c. denotes the complex conjugate. In solving numerically for ϕ_0, ϕ_0^+ and ϕ_{11}, we chose $\phi_0^+(1) = 1$, $\langle \phi_0', \phi_0^{+\prime} \rangle = -p_1 = 1$, and $\phi_{11}''(-1) = 0$. Other normalizations are equally acceptable, their only effect being to change the definition of amplitude (e.g. Herbert 1980).

Similarly, (3.2c) must also satisfy a solvability condition, namely
$$a_T = \mathrm{i}a(\lambda_1^2 (p_2 p_4 - p_5) + c_2 - \lambda_2 p_2 + \alpha_s^2 (p_6 + 2\mathrm{i}\lambda_0) - W p_3 - a\bar{a} p_7), \tag{3.10a}$$
where
$$p_1 p_3 = \langle \tilde{u}_0 \phi_0'', \phi_0^+ \rangle, \quad p_1 p_4 = \langle \phi_{11}'', \phi_0^+ \rangle, \tag{3.10b}$$
$$p_1 p_5 = \mathrm{i} \langle \phi_{11}^{\mathrm{IV}}, \phi_0^+ \rangle, \quad p_1 p_6 = \langle (\hat{u}_0 - c_0) \phi_0, \phi_0^+ \rangle, \tag{3.10c}$$
$$p_1 p_7 = \langle \phi_0 (\phi_{12}'' + \bar{\phi}_{12}'') - \phi_0' (\phi_{12}' + \bar{\phi}_{12}') - \bar{\phi}_0 \phi_{13}'' - \bar{\phi}_0' \phi_{13}' + 2\bar{\phi}_0'' \phi_{13}, \phi_0^{+\prime} \rangle. \tag{3.10d}$$

u_w	$\alpha_c R_c$	u_w	$\alpha_c R_c$
0.48	4363	0.523125	4752
0.51	4570	0.5251	4710
0.51375	4587	0.526875	4507
0.515625	4610	0.527344	4757
0.5175	4607	0.5275	4775
0.519375	4597	0.527844	4772
0.52125	4673	u_w^* asymptote	4771

TABLE 1

With $\mathscr{A} = |a|^2$, (3.10*a*) simplifies to the form

$$\mathscr{A}_T = -\mu_1 \mathscr{A} + \mu_2 \mathscr{A}^2, \tag{3.11a}$$

where

$$\mu_1 = \mu_3 \lambda_1^2 + \mu_4 \alpha_s^2 + \mu_5 W, \tag{3.11b}$$

$$\mu_2 = 2p_7^i, \quad \mu_3 = 2(p_2 p_4^i - p_5^i), \quad \mu_4 = 2(p_6^i + 2\lambda_0), \tag{3.11c}$$

$$\mu_5 = -2p_3^i, \quad \text{and} \quad p_j^i \equiv \mathrm{Im}\,(p_j). \tag{3.11d}$$

The μ_j ($j \geqslant 2$) were calculated for the two cut-off wall velocities identified above, giving for the first mode (M1)

$$\mu_2 = 4288, \quad \mu_3 = 5.924 \times 10^5, \quad \mu_4 = 0.1272, \quad \mu_5 = 0.1370, \tag{3.12a}$$

while for the second (M2)

$$\mu_2 = 1.501 \times 10^{15}, \quad \mu_3 = 2.501 \times 10^{15}, \quad \mu_4 = 1.546 \times 10^{-2}, \quad \mu_5 = 7.82 \times 10^{-3}. \tag{3.12b}$$

Hence all the numerical constants are positive, although they do have significantly different magnitudes.

Linear stability

It follows from (3.11) that, first, the flow is linearly stable if $\mu_1 > 0$ and, secondly, the linear neutral curve is described by

$$\mu_3 \lambda_1^2 + \mu_4 \alpha_s^2 + \mu_5 W = 0. \tag{3.13}$$

The artificial parameter δ can be eliminated here to yield the asymptote

$$R \sim \frac{1}{\alpha \lambda_0} \left\{ 1 \pm \left(\frac{\mu_5 (u_w^* - u_w) - \mu_4 \alpha^2}{\lambda_0^2 \mu_3} \right)^{\frac{1}{2}} \right\}. \tag{3.14}$$

Equation (3.14) is then the approximation for the *whole* neutral curve, valid for $0 \leqslant u_w^* - u_w \ll 1$, $R \gg 1$. Its discriminant cannot be imaginary; consequently the critical Reynolds number, above which the flow is linearly unstable, is given by

$$R_c \sim (\alpha_c \lambda_0)^{-1}, \quad \alpha_c^2 \sim \mu_4^{-1} \mu_5 (u_w^* - u_w). \tag{3.15a,b}$$

This implies that the neutral curve disappears for $u_w > u_w^*$, consistent with the definition of u_w^*. In table 1 and figure 5, Reynolds & Potter's data for $\alpha_c R_c$ and α_c^2 respectively are re-presented, together with the predictions for M1 from (2.7), (3.12*a*) and (3.15). Extrapolation of their data (figure 5) produces $u_w^* = 0.528$, in very good agreement with (2.7*a*). Similar estimates for λ^* and c^* from their data are 2.10×10^{-4} and -0.051 in turn, which again compare favourably with our M1 results in (2.7*a*).

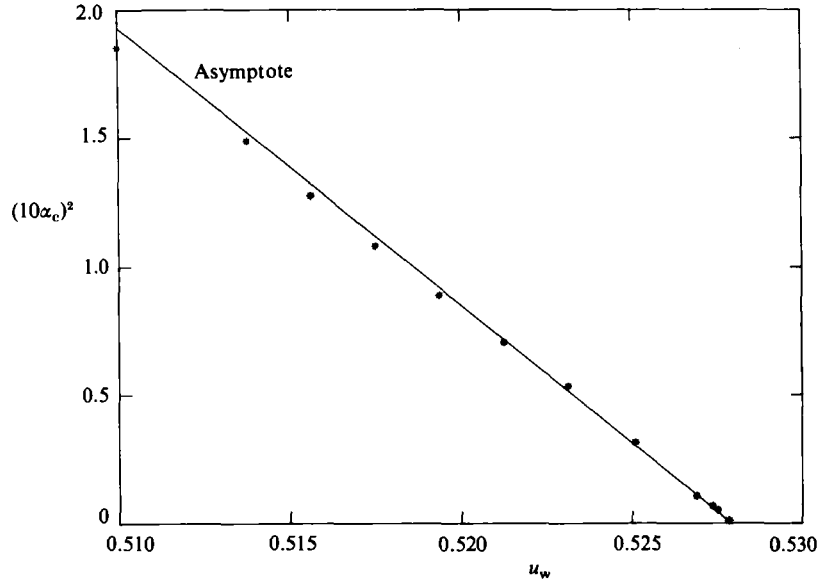

FIGURE 5. Plot of α_c^2 versus u_w for Reynolds and Potters' data (*); ——, asymptote (3.15 *b*).

Weakly nonlinear solutions

Since $\mu_2 > 0$ the finite-amplitude ($\mathscr{A} > 0$) solutions to (3.11), $\mathscr{A} = \mu_1 \mu_2^{-1}$, exist only if $\mu_1 > 0$, i.e. if $\mu_5 W > -(\mu_3 \lambda_1^2 + \mu_4 \alpha_S^2)$. We consider $W < 0$ and $W > 0$ in turn, i.e. $u_w \lessgtr u_w^*$.

(i) $u_w < u_w^*$

Here at all points on the linear neutral curve there is a subcritical bifurcation from the undisturbed-flow solution $\mathscr{A} = 0$. Further, (3.11) shows the finite-amplitude solution to be unstable, representing a threshold amplitude below which disturbances with a specified wavelength decay and above which they grow without bound, on this scale. If we write $A^2 = \delta^2 \mathscr{A}$ to eliminate δ, the nonlinear solutions are, to leading order,

$$\mu_2 A^2 = \mu_3 \left(\frac{1}{\alpha R} - \lambda_0\right)^2 + \frac{\mu_4}{\lambda_0^2 R^2} + \mu_5 (u_w - u_w^*). \tag{3.16}$$

A schematic plot at fixed $R < R_c$ (figure 6) illustrates that, while the amplitude A is small for small variations in wavenumber α from $(\lambda_0 R)^{-1}$, for other α the neutral states will have order-one amplitudes, with the flow then being distinctly different from PPCF. It is not known yet, however, whether the curve of A against α is closed, as in figure 1, for numerical nonlinear solutions are required when $A = O(1)$, e.g. as in Herbert (1976). Similarly (3.1*b*) suggests that the disturbance amplitudes will be order one when R is no longer large, a result of potential significance when the two-dimensional nonlinear critical Reynolds numbers R_G (cf. §1) are sought for *both* the neutral curves M1, M2.

(ii) $u_w > u_w^*$

Here PPCF is linearly stable, but nonlinear solutions still exist, from (3.16), and again represent threshold amplitudes. Rather than bifurcations from a finite R, these

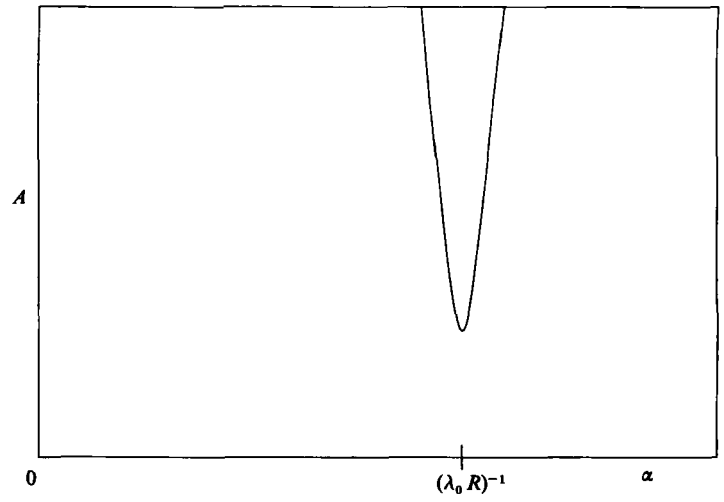

FIGURE 6. Plot of amplitude against wavelength for $R < R_c = (\mu_4/\lambda_0^2\mu_5(u_w^* - u_w))^{\frac{1}{2}}$.

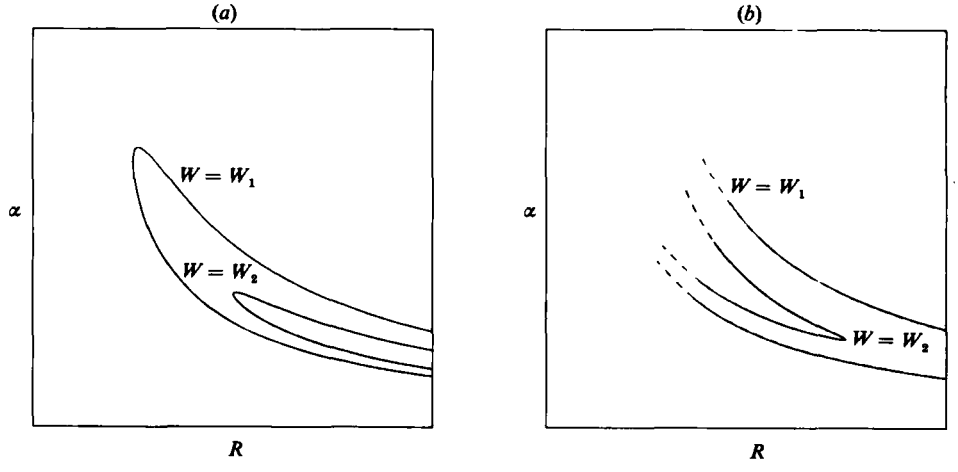

FIGURE 7. Neutral curves. (a) $\mu_j > 0$; $W_1 < W_2 < 0$. (b) $\mu_3 > 0$, $\mu_4 < 0$; $\mu_5 W_1 < 0$, $\mu_5 W_2 > 0$.

solutions can be thought of as 'bifurcations from infinity'. Rosenblat & Davis (1979) conjectured on such bifurcations for CF, while Smith & Bodonyi (1982) found nonlinear solutions that bifurcate from infinity in Hagen–Poiseuille pipe flow. Note that (3.16) implies that when $u_w - u_w^*$ approaches $O(1)$ the flow is no longer a small perturbation of PPCF, supporting the argument (e.g. Rosenblat & Davis 1979) against the approaches of Davey & Nguyen (1971), Ellingsen *et al.* (1970), Coffee (1977) and Itoh (1977) referred to in §1. It is noted also that our minimum amplitude based on the u-perturbation does not fall to zero as $R \to \infty$ (cf. Rosenblat & Davis' model problems), whereas the minimum v-perturbation amplitude does.

Finally, we remark in passing that, when the μ_j are not all positive, (3.11a, b) describe a wider variety of linear neutral curves and their bifurcations. For example, if $\mu_2 < 0$ and $\mu_j > 0$ ($j \neq 2$), then (3.11a, b) again describe a neutral curve that disappears to infinity, but with supercritical bifurcations. In this case *no* solutions

exist for $W > 0$. As another example, suppose that $\mu_3 > 0$, $\mu_4 < 0$. Then (3.11a, b) describe a neutral curve that, instead of 'disappearing' to infinity (figure 7a), 'retreats' from infinity (figure 7b). Hence for $\mu_5 W > 0$ neutral solutions only exist for $\alpha_s > (-\mu_5 W/\mu_4)^{\frac{1}{2}}$.

4. Comments

The first point is that a number of linear neutral curves exist in PPCF. In PPF ($u_w = 0$) there is only one, but as u_w increases two extra neutral curves soon emerge: see Appendix. For u_w slightly larger, but still small, one of these new neutral curves then disappears, whereas the two remaining ones disappear only when u_w is $O(1)$: see §2. We have concentrated on these two main neutral curves. They disappear at u_w values which a study for large R accurately identifies, along with an account of the whole neutral curve then. The inclusion of weak nonlinearity shows the existence of unstable finite-amplitude solutions. These bifurcate subcritically from PPCF for u_w just below the cut-off value u_w^*, whereas for u_w just above u_w^* they 'bifurcate from infinity'. The nonlinear solutions close to the largest u_w^* value are probably of most physical importance with regard to experimental testing. In particular for $u_w \gtrsim \max(u_w^*)$ all disturbances of amplitude A, whatever their wavelength, are likely to decay if

$$A^2 < \frac{1}{\mu_2}\left(\mu_5(u_w - u_w^*) + \frac{\mu_4}{\lambda_0^2 R^2}\right). \tag{4.1}$$

Smith & Bodonyi (1982) also found nonlinear solutions that bifurcate from infinity, in Hagen–Poiseuille pipeflow. For disturbance wavelengths comparable to the pipe radius the pressure perturbation does not have a minimum amplitude, but their analysis suggested that the minimum occurs for wavelengths $O(R)$, with an azimuthal wavenumber $n = 1$. The present analysis can but support this conjecture. Incidentally, however, the 'minimum' threshold amplitude does depend on which amplitude is taken. For example, for the streamwise velocity perturbation Smith & Bodonyi's analysis demonstrates that the minimum threshold amplitude for Hagen–Poiseuille flow occurs for a shorter wavelength, comparable to the pipe radius. Another useful way of viewing the circular-pipe-flow case is to consider instead flow through an elliptical pipe, combining the present approach concerning 'cut-off' with the Hocking (1977) and Davey (1978b) calculations and Smith's (1979) asymptotes, in an attempt to connect with Smith & Bodonyi's findings above. In particular, Davey's calculations suggest $\alpha_c R_c \to$ constant as the cut-off ellipticity is approached.

For u_w (or ellipticities) significantly above a cut-off value, the bifurcation solutions are no longer a small perturbation from the original flow, and a numerical (progressive wave) solution seems necessary, e.g. as in Herbert (1976). Since there are two $O(1)$ cut-off values in PPCF, there may be two such bifurcating solutions eventually, or three counting the third neutral curve in the Appendix. A continued investigation as the flow alters towards CF should prove interesting: for example, two of the bifurcating solutions might 'coalesce' and disappear (cf. figures 3 and 4). Alternatively UB (upper-branch) nonlinear solutions or structure could be sought (cf. Herbert 1976, figure 1) as a part of a study to test whether CF is stable to all nonlinear two-dimensional disturbances. For example, if UB solutions do exist it is possible that, as u_w increases, the closed loop(s), in the plot of wavenumber versus amplitude (figure 1), shrink to a point and disappear.

S.J.C is very grateful to Professors S. Rosenblat and S. H. Davis for stimulating discussions, and we both thank the referees for their helpful comments.

Appendix

Here the asymptotic form of linear neutral disturbances when $u_w \ll 1$ is outlined from analysis similar to Smith's (1979). Details of the lengthy calculations involved are available from the authors. There are four different magnitudes of u_w that need to be examined.

First Regime, $u_w = O(R^{-\frac{3}{7}})$

To leading order, the asymptotic lower-branch neutral solution is unchanged from the PPF three-zoned form (Lin 1955; Reid 1965; Stuart 1963; Smith 1979) until u_w rises to $O(R^{-\frac{3}{7}})$. If

$$\bar{u}_w = R^{\frac{3}{7}} u_w, \tag{A 1}$$

the scaled wavenumber and wavespeed are $\alpha_0 = R^{\frac{1}{7}}\alpha$ and $c_0 = R^{\frac{2}{7}}c$ respectively, and in the core flow

$$(\tilde{u}, \tilde{v}, \tilde{p}) \sim (U_0, R^{-\frac{1}{7}} V_0, R^{-\frac{3}{7}} P_0), \tag{A 2}$$

while in the upper (+) and lower (−) wall layers, with $Y_\pm = R^{\frac{3}{7}}(1 \mp y)$,

$$(\tilde{u}, \tilde{v}, \tilde{p}) \sim (u_\pm, \mp R^{-\frac{3}{7}} v_\pm, R^{-\frac{3}{7}} p_\pm). \tag{A 3}$$

From (A 2), (A 3) and (2.1) the eigenvalue relation is found to be

$$\frac{4\mathrm{i}\alpha_0^3}{5s^2} = \frac{\mathrm{Ai}'(\beta+\gamma)}{\mathscr{K}(\beta+\gamma)} + \frac{\mathrm{Ai}'(\beta-\gamma)}{\mathscr{K}(\beta-\gamma)}, \tag{A 4a}$$

where

$$s = (3\mathrm{i}\alpha_0)^{\frac{1}{3}}, \quad \mathscr{K}(\xi) = \int_\xi^\infty \mathrm{Ai}(\xi)\,\mathrm{d}\xi, \tag{A 4b}$$

$$\beta = -\tfrac{1}{3}sc_0, \quad \gamma = \tfrac{1}{3}s\bar{u}_w, \tag{A 4c}$$

and Ai (ξ) is the Airy function. Alternatively, (A 4a) can be cast in terms of the modified Tietjens function $\mathscr{F}(z)$ (see e.g. Miles 1960):

$$\frac{4(3\alpha_0^7)^{\frac{1}{3}}}{15} = \frac{z_+}{\mathscr{F}(z_+)} + \frac{z_-}{\mathscr{F}(z_-)}, \tag{A 4d}$$

where

$$z_\pm = (\tfrac{1}{9}\alpha_0)^{\frac{1}{3}}(c_0 \pm \bar{u}_w). \tag{A 4e}$$

When $\bar{u}_w = 0$ (A 4d) yields the PPF result $z_+ = z_- = z_0$, where z_0 is the unique root of $\mathrm{Im}(\mathscr{F}(z)) = 0$, but our interest, for the sake of §2, is more in the limit $\bar{u}_w \to \infty$. Three possibilities then exist: (i) z_+ and z_- remain $O(1)$; (ii) $|z_\pm| \to \infty$ with $z_\mp = O(1)$; and (iii) $|z_+|$ and $|z_-| \to \infty$. Each possibility will be considered in turn.

In (i) $\alpha_0 = 9(z_+ - z_-)^3/8\bar{u}_w^3 \to 0$ from (A 4e), and (A 4d) becomes

$$G(z_+, z_-) \equiv \frac{\mathscr{F}(z_+)}{z_+} + \frac{\mathscr{F}(z_-)}{z_-} \sim 0. \tag{A 5}$$

Figure 8 plots Re (G) versus z_+ (given z_-) and z_- (given z_+) when Im (G) = 0. We deduce that $z_+ > 0$, $z_- < 0$ and that there are three roots of $G = 0$. These are

$$(z_-, z_+) \approx (-5.540, 6.135),\ (-4.803, 5.205),\ (-0.893, 2.829), \tag{A 6}$$

with (A 4a) then giving

$$c_0 \bar{u}_w^{-1} \approx 0.0510,\ 0.0401,\ 0.5216 \tag{A 7}$$

respectively as $\bar{u}_w \to \infty$. The current structure breaks down when $\bar{u}_w$ becomes $O(R^{\frac{3}{7}})$ ($u_w = O(1)$), and therefore matches with §2. The three asymptotic forms for $R^{-\frac{3}{7}} \ll u_w \ll 1$,

$$c \sim 0.5216u_w,\ 0.0510u_w,\ 0.0401u_w, \tag{A 8a, b, c}$$

are drawn in figures 3(a), 4(a).

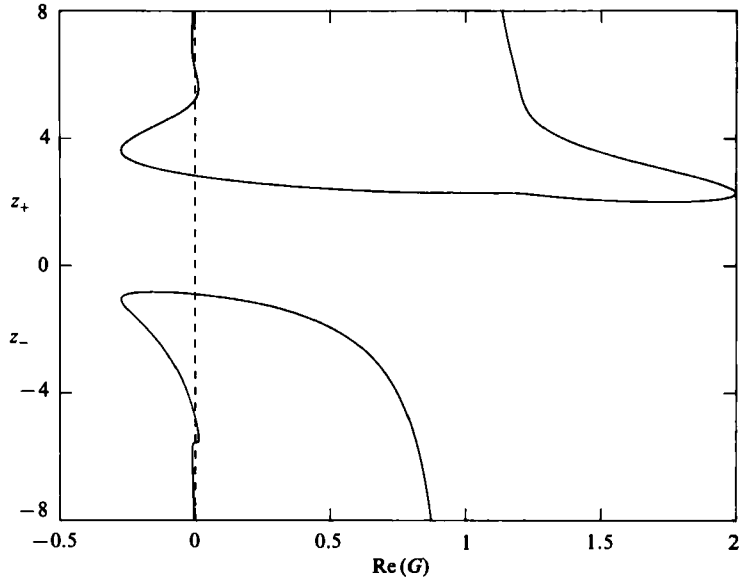

FIGURE 8. Graph of $\mathrm{Re}\,(G(z_+, z_-))$ versus z_+ and z_- for those z_+ and z_- satisfying $\mathrm{Im}\,(G(z_+, z_-)) = 0$; – – –, $\mathrm{Re}\,(G) = 0$.

In (ii) suppose (without loss of generality, because of the symmetry $u_w \to -u_w$) that $z_+ \to \infty$ with $z_- = O(1)$. Since, from Miles (1960),

$$\mathscr{F}(z) \sim 1 + \frac{e^{\frac{1}{4}i\pi}}{z^{\frac{3}{2}}} + \frac{9e^{\frac{1}{2}i\pi}}{4z^3} \quad \text{as } z \to \infty, \tag{A 9}$$

it follows that

$$\left.\begin{aligned} z_- \sim z_0, \quad c_0 \sim \bar{u}_w + \left(\frac{9}{\alpha_0}\right)^{\frac{1}{3}} z_0, \\ \frac{2\alpha_0^2}{5} - \left(\frac{9}{\alpha_0}\right)^{\frac{1}{3}} \frac{z_0}{2}\left(\frac{1}{\mathscr{F}(z_0)} + 1\right) \sim \bar{u}_w. \end{aligned}\right\} \quad \text{as } \bar{u}_w \to \infty. \tag{A 10}$$

Now the structure alters when $\bar{u}_w$ becomes $O(R^{\frac{12}{91}})$, i.e. when u_w is $O(R^{-\frac{2}{13}})$, because a viscous critical layer develops within the lower wall layer. The new structure there is similar, but not identical, to the PPF upper-branch type (see below). Consideration of the regimes $\alpha = O(R^{-\frac{1}{13}})$, $O(R^{-\frac{1}{11}})$ subsequently achieves a match with the upper branch PPF form (see figure 9).

In (iii), if $z_+ \to +\infty$ and $z_- \to -\infty$, then

$$\alpha_0^5 \sim 450\bar{u}_w^{-1}, \quad 2c_0 \sim \alpha_0^2 \quad \text{as } \bar{u}_w \to \infty. \tag{A 11}$$

So the structure fails when $\bar{u}_w$ becomes $O(R^{\frac{10}{133}})$, i.e. when u_w is $O(R^{-\frac{4}{19}})$, owing to a viscous critical-layer/boundary-layer interaction. Unlike other such solutions of this form, there is then no significant pressure variation across the channel.

Second Regime, $u_w = O(R^{-\frac{2}{11}})$

In this upper-branch case the dominant scalings are (Smith 1979)

$$\alpha = \epsilon\alpha_0, \quad c = \epsilon^2 c_0, \quad u_w = \epsilon^2 \bar{u}_w, \tag{A 12}$$

where now $\epsilon = R^{-\frac{1}{11}}$. No direct match with the previous forms is possible, but the regime $u_w = O(R^{-\frac{2}{13}})$ turns up again subsequently. The analysis is very similar to

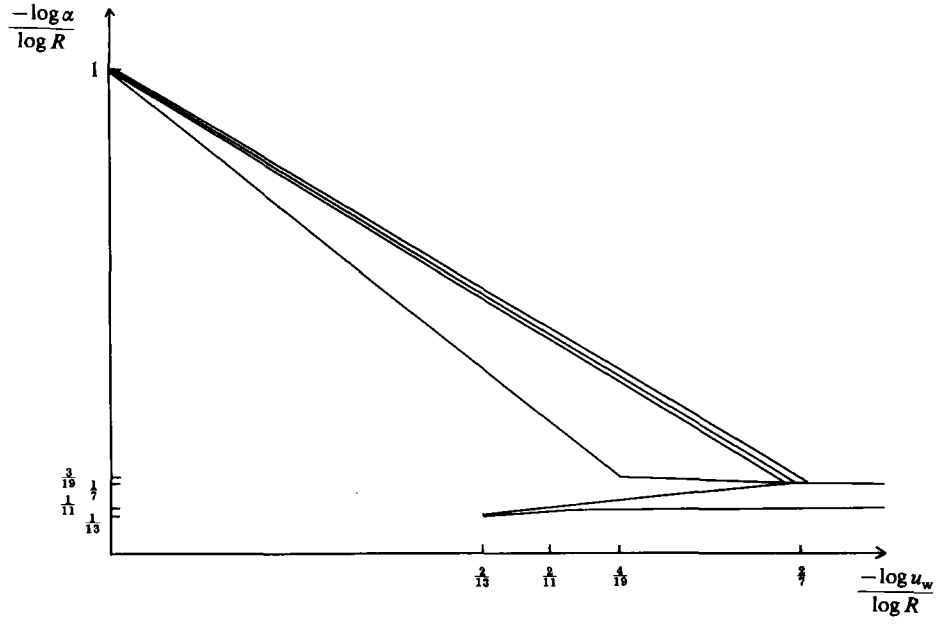

FIGURE 9. Schematic graph of wall velocity versus wavenumber for neutral modes.

Smith (1979), there being seven asymptotic regions. The only significant difference is that it is necessary to consider asymmetric modes. We find the eigenvalue relation

$$c_0 = \tfrac{2}{5}\alpha_0^5, \quad (c_0 - \bar{u}_w)^{-\frac{1}{2}} + (c_0 + \bar{u}_w)^{-\frac{1}{2}} = \tfrac{1}{9}(8\alpha_0)^{\frac{1}{2}}\pi(c_0^2 + \bar{u}_w^2), \qquad \text{(A 13}a,b\text{)}$$

where $c_0 > |\bar{u}_w|$ so that critical layers implicit in the analysis exist. The solution of (A 13) is unique, recovering the PPF result for $\bar{u}_w \to 0$, while as $\bar{u}_w \to \infty$

$$\alpha_0^2 \sim \tfrac{5}{2}\bar{u}_w, \quad c_0 \sim \bar{u}_w + \frac{81}{16\pi^2(10\bar{u}_w^9)^{\frac{1}{2}}}. \qquad \text{(A 14)}$$

This structure breaks down when $\bar{u}_w$ becomes $O(R^{\frac{4}{143}})$, i.e. when u_w is $O(R^{-\frac{2}{13}})$, because the upper critical layer and boundary layer expand into the surrounding 'adjustment' zone and merge. The resulting single zone is of similar structure to the boundary layers for $u_w \approx O(R^{-\frac{2}{7}})$. The following examination of the stage $u_w = O(R^{-\frac{2}{13}})$ demonstrates a link between (A 14) and (A 10).

Third Regime, $u_w = O(R^{-\frac{2}{13}})$

The above subsections suggest the distinct scalings

$$u_w = \epsilon^2\bar{u}_w, \quad (\alpha, c) \sim \epsilon^2(\alpha_0, \bar{u}_w) + \epsilon^4(\alpha_2, c_2), \qquad \text{(A 15)}$$

where now $\epsilon = R^{-\frac{1}{13}}$. As before, there exists a core region and, near the lower wall, an 'adjustment' region within which a critical layer and a viscous wall layer arise. Unusually, the latter's phase lag does not interact with the critical-layer phase jump. Further, the wavespeed is close to the upper wall velocity, and so, instead of an upper 'adjustment' region, there is an upper boundary layer of the $u_w = O(R^{-\frac{2}{7}})$ kind. Hence this mode is like half of the lower branch and half of the upper branch of the PPF form. We find the eigenvalue relations

$$\tfrac{2}{5}\alpha_0^2 = \bar{u}_w, \quad c_2(1 + \mathscr{F}^{-1}(z)) - \tfrac{8}{5}\alpha_0\alpha_2 = \tfrac{16}{75}\alpha_0^4(\tfrac{299}{420} - i\pi + \ln\tfrac{2}{15}\alpha_0^2), \qquad \text{(A 16}a,b\text{)}$$

where $z = (\frac{1}{9}\alpha_0)^{\frac{1}{3}} c_2$. The imaginary part of (A 16b) yields

$$H(z) \equiv \frac{z\,\mathrm{Im}\,(\mathscr{F}(z))}{|\mathscr{F}(z)|^2} = \tfrac{4}{9}\pi\,(\tfrac{45}{2}\bar{u}_{\mathrm{w}}^{13})^{\frac{1}{6}}. \tag{A 16c}$$

From the Tietjens function tabulated in Miles (1960), we deduce that $\bar{u}_{\mathrm{w}} \leqslant \bar{u}_{\mathrm{w}}^*$, where $\bar{u}_{\mathrm{w}}^*$ corresponds to the maximum of H and is the third cut-off wall velocity referred to in the main text. For $\bar{u}_{\mathrm{w}} > \bar{u}_{\mathrm{w}}^*$ there are no neutral modes on this scaling, while for $\bar{u}_{\mathrm{w}} < \bar{u}_{\mathrm{w}}^*$ the upper and lower branches of a neutral curve exist. Further, c_2 and α_2 can be shown to match with (A 10) as $z \to z_0+$ and with (A 14) as $z \to +\infty$. This stage therefore links the previous upper-branch and lower-branch forms, as required and as shown schematically in figure 9.

The one remaining part of figure 9 to consider, near $u_{\mathrm{w}} = O(R^{-\frac{4}{19}})$, $\alpha = O(R^{-\frac{3}{19}})$, is forced by (A 11) and explains how one of the limits for $u_{\mathrm{w}} = O(R^{-\frac{2}{7}})$ becomes an upper branch for $u_{\mathrm{w}} = O(1)$.

Fourth Regime, $u_{\mathrm{w}} = O(R^{-\frac{4}{19}})$

The limit (A 11) suggests the scaling

$$u_{\mathrm{w}} = \epsilon^4 \bar{u}_{\mathrm{w}}, \quad \alpha \sim \epsilon^3\alpha_0 + \epsilon^5\alpha_1 + \epsilon^7 \ln \epsilon\alpha_{2a} + \epsilon^7\alpha_2, \quad c \sim \epsilon^6 c_1 + \epsilon^8 \ln \epsilon c_{2a} + \epsilon^8 c_2, \tag{A 17}$$

where $\epsilon = R^{-\frac{1}{19}}$. The core solution proceeds much as before except that, unusually, the pressure perturbation is constant across the channel. Again there are 'adjustment' zones and viscous boundary layers at the walls, with some slight modifications (e.g. two terms need to be calculated in the boundary layers). The eigenvalue relations, determined by a more complicated interaction than before, are found to be

$$\frac{\alpha_0^2}{10(2\alpha_0\,\bar{u}_{\mathrm{w}})^{\frac{1}{2}}} = \frac{3}{2\alpha_0\,\bar{u}_{\mathrm{w}}} - \frac{\pi\bar{u}_{\mathrm{w}}^3}{36}, \quad c_1 - \frac{2\alpha_0^2}{5} = \frac{3}{(2\alpha_0\,\bar{u}_{\mathrm{w}})^{\frac{1}{2}}}. \tag{A 18}$$

These have a unique solution for all $\bar{u}_{\mathrm{w}}$, matching with (A 11) as $\bar{u}_{\mathrm{w}} \to 0$. For large $\bar{u}_{\mathrm{w}}$

$$\alpha_0 \sim \frac{54}{\pi\bar{u}_{\mathrm{w}}^4}, \quad c_1 \sim (\tfrac{1}{12}\pi\bar{u}_{\mathrm{w}}^3)^{\frac{1}{2}}. \tag{A 19}$$

From the scaling (A 17), (A 19) breaks down when $\bar{u}_{\mathrm{w}}$ becomes $O(R^{\frac{4}{19}})$, i.e. when u_{w} is $O(1)$. For $R^{-\frac{4}{19}} \ll u_{\mathrm{w}} \ll 1$, (A 19) yields the asymptote $c \sim (\frac{1}{12}\pi u_{\mathrm{w}}^3)^{\frac{1}{2}}$ plotted (dash–dot) in figure 4(a).

This completes our examination of the neutral modes when $0 \leqslant u_{\mathrm{w}} \ll 1$, the results being summarized in figure 9. To recapitulate:

(i) $u_{\mathrm{w}} = O(R^{-\frac{2}{7}})$, $\alpha = O(R^{-\frac{1}{7}})$. For this scaling the lower-branch PPF form is changed significantly. For $u_{\mathrm{w}} \ll R^{-\frac{2}{7}}$ there is only one mode, while for $u_{\mathrm{w}} \gg R^{-\frac{2}{7}}$ there are five modes. Three of these modes match directly onto the $u_{\mathrm{w}} = O(1)$, $\alpha = O(R^{-1})$ scaling of §2. The other two modes match onto disturbances with scalings $u_{\mathrm{w}} = O(R^{-\frac{4}{19}})$, $\alpha = O(R^{-\frac{3}{19}})$ and $u_{\mathrm{w}} = O(R^{-\frac{2}{13}})$, $\alpha = O(R^{-\frac{1}{13}})$.

(ii) $u_{\mathrm{w}} = O(R^{-\frac{4}{19}})$, $\alpha = O(R^{-\frac{3}{19}})$. The one mode with this scaling matches onto one of the $u_{\mathrm{w}} = O(R^{-\frac{2}{7}})$ modes and one of the $u_{\mathrm{w}} = O(1)$ modes.

(iii) $u_{\mathrm{w}} = O(R^{-\frac{2}{11}})$, $\alpha = O(R^{-\frac{1}{11}})$. For this scaling there are two modes with significantly different structures. One of them can be viewed as the 'large' u_{w} limit of a $u_{\mathrm{w}} = O(R^{-\frac{2}{7}})$ mode. The other mode is the 'continuation' of the upper-branch PPF mode. Both modes match onto disturbances with scalings $u_{\mathrm{w}} = O(R^{-\frac{2}{13}})$, $\alpha = O(R^{-\frac{1}{13}})$.

(iv) $u_{\mathrm{w}} = O(R^{-\frac{2}{13}})$, $\alpha = O(R^{-\frac{1}{13}})$. There is a third cut-off wall velocity on this scale, above which no modes exist. For $u_{\mathrm{w}} \ll R^{-\frac{2}{13}}$ the two modes match as discussed above.

The structure of these modes is similar to the lower-branch PPF mode adjacent to one wall, and the upper branch PPF mode adjacent to the other.

Finally we note that there is one neutral curve for $u_w \lesssim R^{-\frac{1}{7}}$, there are three neutral curves for $R^{-\frac{1}{7}} \lesssim u_w \lesssim R^{-\frac{4}{13}}$, and two for $R^{-\frac{4}{13}} \lesssim u_w \ll 1$. There may also be a range of u_w of $O(R^{-\frac{1}{7}})$ where there are two neutral curves.

REFERENCES

CHEN, T. S. & JOSEPH, D. D. 1973 Subcritical bifurcation of plane Poiseuille flow. *J. Fluid Mech.* **58**, 337–351.

COFFEE, T. 1977 Finite-amplitude instability of plane Couette flow. *J. Fluid Mech.* **83**, 401–414.

DAVEY, A. 1978*a* On Itoh's amplitude stability theory for pipe flow. *J. Fluid Mech.* **86**, 695–703.

DAVEY, A. 1978*b* On the stability of flow in an elliptic pipe which is nearly circular. *J. Fluid Mech.* **87**, 233–241.

DAVEY, A. & NGUYEN, H. P. F. 1971 Finite-amplitude stability of pipe flow. *J. Fluid Mech.* **45**, 701–720.

ELLINGSEN, T., GJEVICK, B. & PALM, E. 1970 On the nonlinear stability of plane Couette flow. *J. Fluid Mech.* **40**, 97–112.

HAINS, F. D. 1967 Stability of plane Couette–Poiseuille flow. *Phys. Fluids* **10**, 2079–2080.

HEISENBERG, W. 1924 Über Stabilität und Turbulenz von Flüssigkeitsströmen. *Ann. der Phys.* **74**, 577–627.

HERBERT, T. 1976 Periodic motions in a plane channel. In *Proc. 5th Intl Conf. on Numerical Methods in Fluid Dynamics* (ed. A. I. van de Vooren & P. J. Zandbergen). Lecture Notes in Physics, vol. 59. Springer.

HERBERT, T. 1977 Die neutrale Fläche der ebenen Poiseuille-Strömung. Habilitationsschrift, Universität Stuttgart.

HERBERT, T. 1980 Nonlinear stability of parallel flows by high-order amplitude expansions. *AIAA J.* **18**, 243–248.

HERBERT, T. 1981*a* Stability of plane Poiseuille flow. Theory and experiment. In *Proc. XV Symp. on Advanced Problems and Methods in Fluid Mechanics, Jachranka, Poland.* See also *Fluid Dyn. Trans.* **11** (1983), 77–126, and VPI-E-81-35.

HERBERT, T. 1981*b* A secondary instability mechanism in plane Poiseuille flow. *Bull. Am. Phys. Soc.* **26**, 1257.

HERBERT, T. 1983*a* Secondary instability of plane channel flow to subharmonic three-dimensional disturbances. *Phys Fluids* **26**, 871–874.

HERBERT, T. 1983*b* Subharmonic three-dimensional disturbances in unstable plane shear flows. *AIAA*-83-1759.

HOCKING, L. M. 1977 The stability of flow in an elliptic pipe with large aspect ratio. *Q. J. Mech. Appl. Maths* **30**, 343–353.

ITOH, N. 1977 Nonlinear stability of parallel flows with subcritical Reynolds numbers. Part 1. An asymptotic theory valid for small-amplitude disturbances. *J. Fluid Mech.* **82**, 455–467.

LIN, C. C. 1945 On the stability of two-dimensional parallel flows. *Q. Appl. Maths* **3**, 117–142, 218–234, 277–301.

LIN, C. C. 1955 *The Theory of Hydrodynamic Stability.* Cambridge University Press.

MACKRODT, P.-A. 1976 Stability of Hagen–Poiseuille flow with superimposed rigid rotation. *J. Fluid Mech.* **73**, 153–164.

MEKSYN, D. & STUART, J. T. 1951 Stability of viscous motion between parallel planes for finite disturbances. *Proc. R. Soc. Lond.* A **208**, 517–526.

MILES, J. W. 1960 The hydrodynamic stability of a thin film of liquid in uniform shearing motion. *J. Fluid Mech.* **8**, 593–610.

ORSZAG, S. A. 1971 Accurate solution of the Orr–Sommerfeld stability equation. *J. Fluid Mech.* **50**, 689–703.

ORSZAG, S. A. & KELLS, L. C. 1980 Transition to turbulence in plane Poiseuille and plane Couette flow. *J. Fluid Mech.* **96**, 159–206.

ORSZAG, S. A. & PATERA, A. T. 1980 Subcritical transition to turbulence in plane channel flows. *Phys. Rev. Lett.* **45**, 989–993.

POTTER, M. C. 1966 Stability of plane Couette–Poiseuille flow. *J. Fluid Mech.* **24**, 609–619.

REID, W. H. 1965 The stability of parallel flows. In *Basic Developments in Fluid Dynamics*, vol. 1 (ed. M. Holt). Academic.

REYNOLDS, W. C. & POTTER, M. C. 1967 Finite-amplitude instability of parallel shear flows. *J. Fluid Mech.* **27**, 465–492.

ROMANOV, V. A. 1973 Stability of plane-parallel Couette flow. *Funct. Anal. Applics* **7**, 137–146.

ROSENBLAT, S. & DAVIS, S. H. 1979 Bifurcation from infinity. *SIAM J. Appl. Maths* **37**, 1–19.

SMITH, F. T. 1974 Boundary layer flow near a discontinuity in wall conditions. *J. Inst. Maths Applics* **13**, 127–145.

SMITH, F. T. 1979 Instability of flow through pipes of general cross-section. Parts I and II. *Mathematika* **26**, 187–210, 211–223.

SMITH, F. T. & BODONYI, R. J. 1982 Amplitude-dependent neutral modes in the Hagen–Poiseuille flow through a circular pipe. *Proc. R. Soc. Lond.* A **384**, 463–489.

SMITH, F. T., PAPAGEORGIOU, D. & ELLIOTT, J. W. 1984 An alternative approach to linear and nonlinear stability calculations at finite Reynolds numbers. *J. Fluid Mech.* **146**, 313–330.

STEWARTSON, K. & STUART, J. T. 1971 A nonlinear instability theory for a wave system in plane Poiseuille flow. *J. Fluid Mech.* **48**, 529–545.

STUART, J. T. 1960 On the non-linear mechanics of wave disturbances in stable and unstable parallel flows. Part 1. *J. Fluid Mech.* **9**, 353–370.

STUART, J. T. 1963 Hydrodynamic stability. In *Laminar Boundary Layers* (ed. L. Rosenhead). Clarendon.

STUART, J. T. 1981 Instability and transition in pipes and channels. In *Transition and Turbulence* (ed. R. E. Meyer). Academic.

ZAHN, J.-P., TOOMRE, J., SPIEGEL, E. A. & GOUGH, D. O. 1974 Nonlinear cellular motions in Poiseuille channel flow. *J. Fluid Mech.* **64**, 319–345.